Locally periodically poled LNOI ridge waveguide for second harmonic generation [Invited]

Biao Mu (沐 彪)[1], Xianfang Wu (吴先方)[1], Yunfei Niu (钮云飞)[1], Yan Chen (陈 琰)[1], Xinlun Cai (蔡鑫伦)[2],
Yanxiao Gong (龚彦晓)[1], Zhenda Xie (谢臻达)[1], Xiaopeng Hu (胡小鹏)[1*], and Shining Zhu (祝世宁)[1]

[1] National Laboratory of Solid State Microstructures, College of Engineering and Applied Sciences, College of Electronic Science and Engineering, and School of Physics, Nanjing University, Nanjing 210093, China

[2] State Key Laboratory of Optoelectronic Materials and Technologies and School of Electronics and Information Technology, Sun Yat-sen University, Guangzhou 510275, China

*Corresponding author: xphu@nju.edu.cn

Periodically poled lithium niobate on insulator (LNOI) ridge waveguides are desirable for high-efficiency nonlinear frequency conversions, and the fabrication process of such waveguides is crucial for device performance. In this work, we report fabrication and characterization of locally periodically poled ridge waveguides. Ridge waveguides were fabricated by dry etching, and then the high-voltage pulses were applied to locally poled ridge waveguides. Second harmonic generation with normalized conversion efficiency of 435.5% $W^{-1} \cdot cm^{-2}$ was obtained in the periodically poled LNOI ridge waveguide, which was consistent with the triangular domain structure revealed by confocal microscopy.

Keywords: lithium niobate on insulator; ridge waveguide; ferroelectric domain inversion; second harmonic generation.
DOI: 10.3788/COL202119.060007

1. Introduction

In recent years, the lithium niobate (LiNbO₃) on insulator (LNOI) platform has drawn significant interest in the area of integrated photonics. LNOI thin film inherits the outstanding optical properties of LiNbO₃ single crystals, such as a wide transparency window spanning from the visible to mid-infrared, a strong second-order nonlinear coefficient[1], and a high electro-optic coefficient[2]. Furthermore, LNOI possesses a higher refractive index contrast, which is ∼0.7, compared to the conventional weakly confining LiNbO₃ waveguides, such as proton exchange waveguides and titanium in-diffused waveguides[3,4]. Thus, the LNOI platform enables a stronger optical confinement, which can enhance the light–matter interaction, thus lowering the power consumption and improving the integration density for photonic devices. Because of the above advantages, LNOI has been used to construct a variety of photonic devices, such as high-speed electro-optic modulators[5,6], high-speed acousto-optic modulators[7], high-efficiency nonlinear frequency converters[8–10], high-Q micro-disk resonators[11–13], and photonic crystal micro-cavities[14].

Among the photonic devices, nonlinear frequency converters based on the quasi-phase-matching (QPM) technique are of particular interest. QPM has some advantages over other methods such as realizing phase-matching of arbitrary second-order

nonlinear processes and utilizing the largest second-order nonlinear coefficient d_{33}. To date, periodically poled LNOI (PPLNOI) waveguides have been fabricated to realize QPM second-order nonlinear processes, such as ultra-high-efficiency second harmonic generation (SHG)[15–17], sum-frequency generation (SFG)[18,19], difference frequency generation (DFG)[15], and high-brightness entangled photons generation through spontaneous parametric down conversion (SPDC)[20]. To obtain LNOI photonic devices with ferroelectric domain inversion, the commonly used procedure is electrical field poling followed by inductively coupled plasma (ICP) dry etching. However, extra loss will be introduced in the dry-etching process due to the uneven waveguide side walls caused by the different etching rates of the positive and negative domains[21]. Differential etching occurs not only in the dry-etching process, but also in other processes such as thinning periodically poled LiNbO₃ crystals using the chemical mechanical polishing technique[22].

In this work, we investigate an alternative process for fabrication of ferroelectric domain structures in X-cut LNOI, which is the local periodical poling of the thin film LiNbO₃ ridge waveguide. Electrical poling with in-plane patterned electrodes was exploited to realize domain inversion in a dry-etched ridge waveguide. The frequency doubling performances of the fabricated nonlinear waveguide were characterized and analyzed in theory.

2. Fabrication

The devices were fabricated on an LNOI chip (NANOLN) with a 600-nm-thick X-cut LiNbO$_3$ thin film. The fabrication process could be divided into two stages. The waveguides were formed on the sample by the dry etching method, and then the ferroelectric domain structure in the waveguides was obtained using the electric field poling technique. The specific steps are shown in Fig. 1(a). Firstly, ridge waveguides were fabricated by using electron beam lithography (EBL) and an ICP-etching process. The geometry of the ridge waveguides is shown in Fig. 1(b). The top width of the waveguides was 2.3 μm, and the etching depth was about 350 nm. Besides, the sidewall angle of the waveguides was about 60°. Secondly, a comb-slab-shaped metal electrode was deposited on both sides of the ridge waveguides. The geometry of the electrodes is schematically shown in Fig. 1(c). The period of the patterned electrodes was 4.5 μm, and the spacing between the in-plane positive and negative electrodes was 2.3 μm. After this, several high-voltage pulses are applied to the electrodes to

obtain periodic inverted domain structures defined by the patterned electrodes. The length of the poled waveguide was 6 mm. After the periodic poling process, the electrodes were removed. The waveguide facets were exposed by incising the chip, and they were polished by a focused ion beam (FIB) etching process. Figure 1(d) shows the scanning electron microscope (SEM) image of the ridge waveguide after poling, and we can see that the sidewall surface is smooth, which indicates that the fabrication procedure, i.e., poling after etching, will not introduce extra loss to the waveguide. The propagation loss of the ridge waveguide was measured to be about 1.0 dB/cm by using the Fabry–Perot (F-P) method.

Conventional electric field poling technology was applied to obtain the periodical domain structure in the LNOI ridge waveguide. The coercive field of the X-cut LNOI is about 30 kV/mm[17], which is higher than that that of the bulk LiNbO$_3$ crystal (∼21 kV/mm). This characteristic requires a higher poling voltage for domain inversion in LiNbO$_3$ thin films. In the ferroelectric domain structure fabricating process, the applied poling voltage was 3.6 times that of the coercive field of the X-cut thin film, and the pulse duration was set to be 10 ms. Several high-voltage pulses were applied to the electrodes deposited on the LNOI chip to obtain the domain inversion. After the electric poling process, confocal second harmonic (SH) microscopy was used to non-destructively characterize the inverted ferroelectric domain structure. The recorded domain structure is shown in Fig. 2(a), and the area surrounded by the red dashed square in Fig. 2(a) is the inverted domain area. From the figure, we can see that the inverted domains from the combed electrode were not extended sufficiently to the slab electrode, and they exhibit an inversed triangle shape. To investigate the inversed domain shape, we simulate the electric field distribution at the waveguide surface viewing from the top and the transverse electric (TE) field profile, as shown in Figs. 2(b) and 2(c),
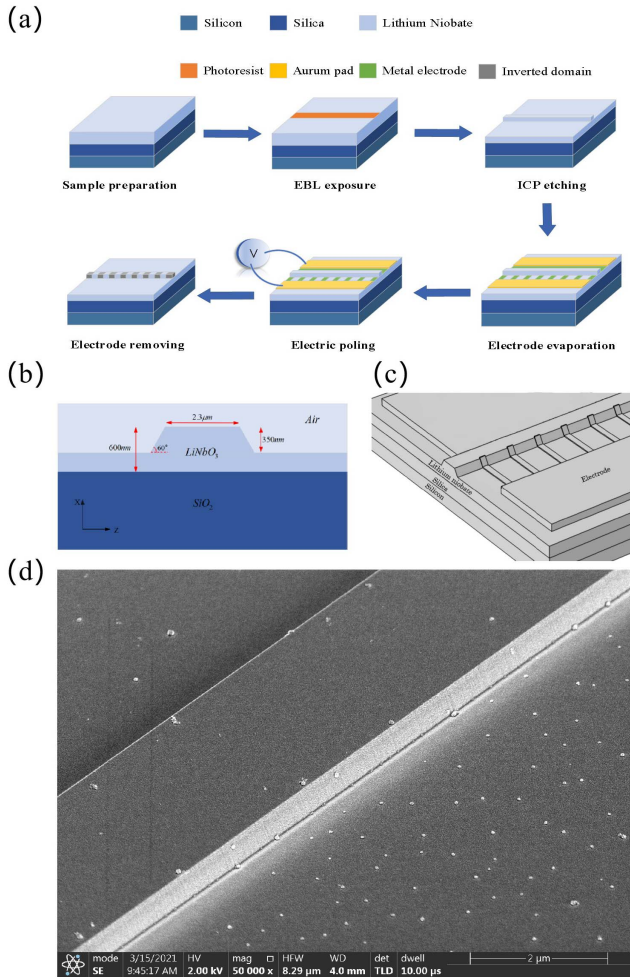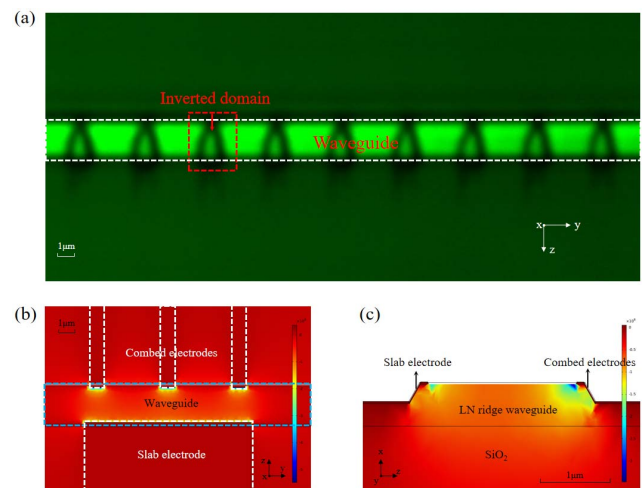

Fig. 1. (a) Fabrication steps of the periodically poled LNOI ridge waveguide. (b) Geometric schematic of the LNOI ridge waveguide cross section. (c) Schematic of the electrode structure on the ridge waveguide. (d) SEM image of the sidewall surface of the ridge waveguide after poling.

Fig. 2. (a) Image of the inverted domain structure of the LNOI ridge waveguide recorded using the confocal SH microscopy. (b) Simulated electric field distribution at the waveguide surface viewing from the top. (c) Simulated transverse electric field profile.

respectively. Due to the small spacing between the positive and negative electrodes, the electric field is concentrated around the tips of the combed electrode and spreads very quickly. The triangular inverted domain structure may be attributed to the highly non-uniform electric field distribution.

3. Experiment and Discussion

The schematic of the experimental setup for characterizing the SHG performance is shown in Fig. 3. The fundamental wave (FW) from a continuous-wave (CW) fiber laser (SANTECH, TSL-550) was gathered into a single-mode fiber. Then, the FW propagated through a polarization controller, which ensured the excitation of the TE mode of the FW in the nano-waveguide. The polarized FW beam was coupled into the thin film ridge waveguide with a lensed fiber, and the fiber-to-chip coupling loss was ~10.5 dB. The output lights were coupled out from the waveguide using an aspherical mirror with an effective focal length of 4.6 mm, and the coupling loss off the chip was ~1 dB. The residual FW and the generated SH wave were separated with a beam splitter, and the powers of two beams were measured, respectively, by two power meters.

In the experiment, we tuned the wavelength of the CW fiber laser from 1400 to 1430 nm to find the QPM wavelength of the nonlinear waveguide. At 1406 nm, a maximum output power of 0.83 µW for the SH wave was obtained, and the corresponding power of the FW was 1.08 mW. The normalized SHG conversion efficiency of the 6-mm-long nonlinear waveguide was calculated to be 435.5% $W^{-1} \cdot cm^{-2}$, which was about one-tenth that of the theoretical value 4326.7% $W^{-1} \cdot cm^{-2}$ in an ideally periodically poled waveguide with 50% duty cycle. The dramatic reduction of the SHG conversion efficiency may be attributed to the triangular domain structure, as shown in Fig. 2(a). The LNOI ridge waveguide was locally periodically poled; however, the shape of the inverted domains was triangular. Thus, the theoretical efficiency derived by using the perfect 50% duty cycle of each point along the Y axis on the waveguide as the theoretical model is inapplicable. To investigate the SHG in the nonlinear waveguide with an irregular domain structure, we start with the equation that describes the SHG[23]:

$$A_2 = i\frac{2\omega_1}{cn_2}A_1^2 \iiint\limits_{\Delta y=L} d^{(2)}(x,y,z)E_f^2 E_s^* e^{-i\Delta\beta y}\mathrm{d}x\mathrm{d}y\mathrm{d}z, \quad (1)$$

where A_1 and A_2 are the field amplitudes of the FW and SH wave; E_f and E_s are the normalized electrical fields of the FW

and SH wave, which can be described as $\iint E_{f,s}^2 \mathrm{d}x\mathrm{d}z = 1$; $\Delta\beta$ is the wave vector mismatch for SHG; L is the interaction length in the propagation direction; $d^{(2)}(x,y,z)$ is the effective second-order nonlinear coefficient; c is velocity of light in vacuum; ω_1 is the frequency of FW; n_2 is the effective refractive index of the SH wave. Because the change period of the effective second-order nonlinear coefficient corresponds to the poling period, the effective second-order nonlinear coefficient can be written as

$$d^{(2)}(x,y,z) = d^{(2)}(x, y+\Lambda, z), \quad (2)$$

with Λ being the poling period. Then, Eq. (1) can be re-written into

$$A_2 = i\frac{2\omega_1}{cn_2}A_1^2 \iiint\limits_{\Delta y=\Lambda} d^{(2)}(x,y,z)E_f^2 E_s^* e^{-i\Delta\beta y}\mathrm{d}x\mathrm{d}y\mathrm{d}z \cdot \mathrm{sinc}\left(\frac{\Delta\beta' L}{2}\right), \quad (3)$$

in which N is the number of the inverted domains; $\Delta\beta'$ is the wave vector mismatch for the FW, the SH wave, and the reciprocal lattice vector provided by ferroelectric domains. The variation of $d^{(2)}(x,y,z)$ over a poling period is related to the shapes of the positive and negative domains within a poling period. Figure 4 shows the schematic of the inverted domain in the LNOI ridge waveguide, and the white triangles indicate the inverted domains. In Fig. 4, a is the half-length of the base of the triangle, b is the height of the triangle, and w is the width of the waveguide. The positive direction of the y axis indicates the propagation direction of the interacting waves. Then, the function $d^{(2)}(x,y,z)$ in one poling period can be expressed as

$$d^{(2)}(x,y,z) = d_{33}\mathrm{sign}\left(\frac{|y|}{a} + \frac{|z|}{b} - 1\right). \quad (4)$$

Subsequently, we can obtain the function $d^{(2)}(x,y,z)$ in the whole waveguide area:

$$d^{(2)}(x,y,z) = d_{33}\mathrm{sign}\left[\frac{|y - \mathrm{floor}(y/\Lambda + 1/2)\Lambda|}{a} + \frac{|z|}{b} - 1\right]. \quad (5)$$
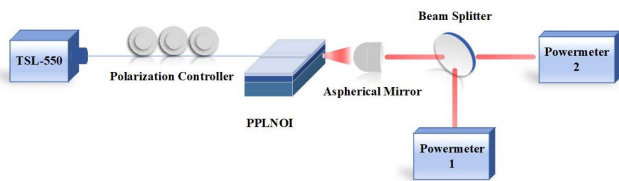

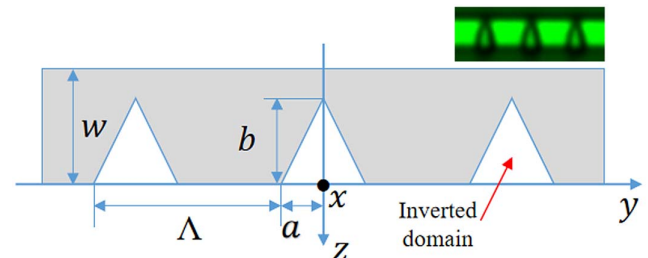Fig. 3. Schematic experimental setup

Fig. 4. Schematic of the inverted domain with triangular shape in the locally periodically poled LNOI ridge waveguide.
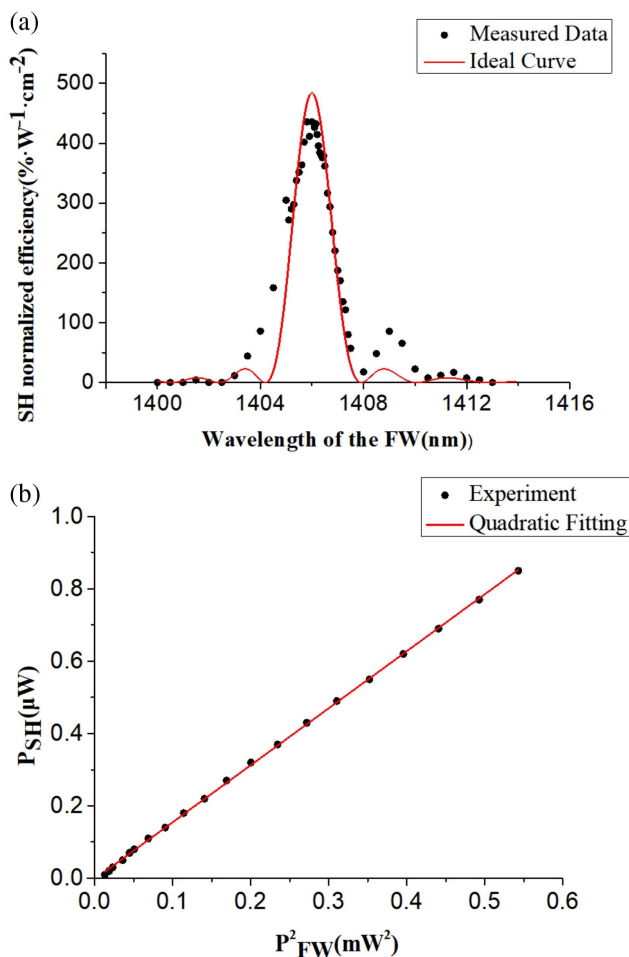
Fig. 5. (a) Measured (black dots) and theoretical (red line) wavelength tuning curves for SHG in the nonlinear waveguide. (b) Quadratic power dependence of the SH wave on the FW. The black dots and the red line are the measured data and the fitting curve, respectively.

According to the recorded domain structure in Fig. 2(a), a and b were, respectively, measured to be nearly 0.63 and 1.83 μm. Thus, the normalized SHG conversion efficiency corresponding to the actual inverted domain structure was calculated to be 484.5% $W^{-1} \cdot cm^{-2}$, which is consistent with the measured one.

The measured and theoretical corrected curves of normalized SHG efficiency depending on the wavelength of the FW are shown in Fig. 5(a). The full width at half-maximum (FWHM) of the wavelength tuning curve was ~2 nm. Figure 5(b) shows the relationship between the SH wave and the square of the power of the FW, which is a linear relation in theory. The red curve is obtained by the quadratic fitting of the experimental results. Using the fitted slope, the normalized SHG conversion efficiency was calculated to be 437.5% $W^{-1} \cdot cm^{-2}$.

4. Conclusion

To conclude, we have fabricated locally periodically poled LNOI ridge waveguides using the following fabrication procedure: dry etching to form the ridge waveguide followed by electrical field poling to obtain ferroelectric domain inversion. The fabricated ridge waveguide was 6-mm-long, and the poling period was 4.5 μm. The performance of the quasi-phase-matched SHG at around 1406 nm in the PPLNOI ridge waveguide was characterized. The normalized SHG conversion efficiency was measured to be 435.5% $W^{-1} \cdot cm^{-2}$, which was in accordance with our theoretical analysis according to the triangular domain structure revealed by the SH confocal microscopy. In addition, the wavelength tuning curve and the output power dependence on the input power of the FW were investigated. To further improve the qualities of the inverted domain structure, we will focus on choosing the appropriate electric field distribution and optimizing the poling parameters, such as the amplitude of the applied voltage, the pulse duration, and the number of pulses.

References

1. K.-K. Wong, *Properties of Lithium Niobate* (Institution of Engineering and Technology, 2002).
2. E. H. Turner, "High-frequency electro-optic coefficients of lithium niobate," Appl. Phys. Lett. **8**, 303 (1966).
3. Y. F. Niu, L. Yang, D. J. Guo, Y. Chen, X. Y. Li, G. Zhao, and X. P. Hu, "Efficient 671 nm red light generation in annealed proton-exchanged periodically poled LiNbO₃ waveguides," Chin. Opt. Lett. **18**, 111902 (2020).
4. M. Bazzan and C. Sada, "Optical waveguides in lithium niobate: recent developments and applications," Appl. Phys. Rev. **2**, 040603 (2015).
5. M. He, M. Xu, Y. Ren, J. Jian, Z. Ruan, Y. Xu, S. Gao, S. Sun, X. Wen, L. Zhou, L. Liu, C. Guo, H. Chen, S. Yu, L. Liu, and X. Cai, "High-performance hybrid silicon and lithium niobate Mach–Zehnder modulators for 100 Gbit s⁻¹ and beyond," Nat. Photon. **13**, 359 (2019).
6. C. Wang, M. Zhang, X. Chen, M. Bertrand, A. Shams-Ansari, S. Chandrasekhar, P. Winzer, and M. Lončar, "Integrated lithium niobate electro-optic modulators operating at CMOS-compatible voltages," Nature **562**, 101 (2018).
7. Z. Yu and X. Sun, "Acousto-optic modulation of photonic bound state in the continuum," Light: Sci. Appl. **9**, 1 (2020).
8. C. Wang, C. Langrock, A. Marandi, M. Jankowski, M. Zhang, B. Desiatov, M. M. Fejer, and M. Lončar, "Ultrahigh-efficiency wavelength conversion in nanophotonic periodically poled lithium niobate waveguides," Optica **5**, 1438 (2018).
9. J. Lin, F. Bo, and Y. Cheng, "Advances in on-chip photonic devices based on lithium niobate on insulator," Photon. Res. **8**, 1910 (2020).
10. A. Boes, L. Chang, and M. Knoerzer, "Improved second harmonic performance in periodically poled LNOI waveguides through engineering of lateral leakage," Opt. Express **27**, 23919 (2019).
11. M. Zhang, C. Wang, R. Cheng, A. Shams-Ansari, and M. Lončar, "Monolithic ultra-high-Q lithium niobate microring resonator," Optica **4**, 1536 (2017).

12. R. Wu, J. Zhang, N. Yao, W. Fang, L. Qiao, Z. Chai, J. Lin, and Y. Cheng, "Lithium niobate micro-disk resonators of quality factors above 107," Opt. Lett. **43**, 4116 (2018).

13. Y. C. Jia, L. Wang, and F. Chen, "Ion-cut lithium niobate on insulator technology: recent advances and perspectives," Appl. Phys. Rev. **8**, 011307 (2021).

14. L. Wang, C. Wang, J. Wang, F. Bo, M. Zhang, Q. Gong, M. Lončar, and Y. F. Xiao, "High-Q chaotic lithium niobate microdisk cavity," Opt. Lett. **43**, 2917 (2018).

15. Y. Niu, C. Lin, X. Liu, Y. Chen, X. Hu, Y. Zhang, X. Cai, Y.-X. Gong, Z. Xie, and S. Zhu, "Optimizing the efficiency of a periodically poled LNOI waveguide using in situ monitoring of the ferroelectric domains," Appl. Phys. Lett. **116**, 101104 (2020).

16. A. Rao, K. Abdelsalam, T. Sjaardema, A. Honardoost, G. F. Camacho-Gonzalez, and S. Fathpour, "Actively-monitored periodic-poling in thin-film lithium niobate photonic waveguides with ultrahigh nonlinear conversion efficiency of 4600% $W^{-1}cm^{-2}$," Opt. Express **27**, 25920 (2019).

17. L. Chang, Y. Li, N. Volet, L. Wang, J. Peters, and J. E. Bowers, "Thin film wavelength converters for photonic integrated circuits," Optica **3**, 531 (2016).

18. G. Li, Y. Chen, H. Jiang, and X. Chen, "Broadband sum-frequency generation using d_{33} in periodically poled $LiNbO_3$ thin film in the telecommunications band," Opt. Lett. **42**, 939 (2017).

19. D. Wang, T. Ding, Y. Zheng, and X. Chen, "Cascaded sum-frequency generation and electro-optic polarization coupling in the PPLNOI ridge waveguide," Opt. Express **27**, 15283 (2019).

20. J. Y. Chen, Y. Meng Sua, Z. H. Ma, C. Tang, Z. Li, and Y-P. Huang, "Efficient parametric frequency conversion in lithium niobate nanophotonic chips," OSA Continuum **2**, 2914 (2019)

21. A. Rao, M. Malinowski, A. Honardoost, J. R. Talukder, P. Rabiei, P. Delfyett, and S. Fathpour, "Second-harmonic generation in periodically-poled thin film lithium niobate wafer-bonded on silicon," Opt. Express **24**, 29941 (2016).

22. M. Wang, R. Wu, J. Lin, J. Zhang, Z. Fang, Z. Chai, and Y. Cheng, "Chemo-mechanical polish lithography: a pathway to low loss large-scale photonic integration on lithium niobate on insulator," Quantum Eng. **1**, e9 (2019).

23. R. W. Boyd, *Nonlinear Optics*, 3rd ed. (Academic, 2008).